Geosynthetics: Leading the Way to a Resilient Planet – Biondi et al (eds)
© 2024 The Author(s), ISBN 978-1-003-38688-9
Open Access: www.taylorfrancis.com, CC BY-NC-ND 4.0 license

Model tests on soil foundation reinforced by geosynthetic encased granular columns subjected to reverse fault movement

J. Chiang & K.-H. Yang
National Taiwan University, Taipei, Taiwan

J.G. Zornberg
The University of Texas at Austin, Texas, USA

E.E. Michel & C.-W. Wu
National Taiwan University, Taipei, Taiwan

ABSTRACT: This paper conducts a 1g model test on soil foundations reinforced by geosynthetic encased granular columns (GECs) across a reverse fault. The aim is to evaluate the effectiveness and reinforcing mechanism of GEC foundations in mitigating the ground surface deformation associated with reverse faulting. For comparison, 1g model tests were also performed on unreinforced and GRS foundations. The test results indicate that GEC foundations can effectively mitigate the ground surface deformation induced by reverse fault movement; compared with the unreinforced foundation, the GEC foundations can reduce the maximum angular distortion at the ground surface by 23.3%–55.6%. A percentage reduction for maximum angular distortion of 23.3% was achieved as the fault offset reached 30% of the foundation height, which mitigates the risk of the surface fault hazards associated with large reverse fault movement.

1 INTRODUCTION

Geosynthetics have been applied in engineering practice to mitigate surface faulting hazards. In central Taiwan, a highway embankment was constructed across the Chelungpu Fault. In the 1999 Chi-Chi earthquake (M_L = 7.3), the vertical surface movement of the Chelungpu Fault reached 2–4 m on average (Chen *et al*. 2001), which resulted in the severe failure of the overlying buildings and infrastructure. The failure of rigid gravity retaining walls was also observed because of the considerable surface rupturing induced by the fault movement. To reduce the risk of a similar event, the Chelungpu Fault was crossed by constructing a ductile highway embankment comprising a geosynthetic-reinforced soil (GRS) wall overlying a GRS foundation.

Yang *et al*. (2020) conducted a series of 1g model tests for investigating the performance of GRS foundations subjected to normal fault movement. The test results revealed that GRS foundations can reduce the fault-induced angular distortion at the ground surface by up to 60% in comparison with unreinforced foundations; this reduction is attributed to the development of the reinforcement tensioned membrane and shear rupture interception effects. Chiang *et al*. (2022) conducted numerical studies to develop design methods for GRS foundations against reinforcement breakage and significant pullout when subjected to normal fault movement. Although studies have validated the benefits of using GRS foundations to mitigate normal fault hazards, the performance of GRS foundations subjected to reverse fault movement has not been understood. Furthermore, GRS foundations might have poor

 DOI: 10.1201/9781003386889-138

effectiveness for reducing reverse fault-induced ground deformation because tensile force is not expected to develop in the reinforcement as the hanging wall moves upward. Another type of reinforced foundation, soil foundation reinforced by geosynthetic encased granular columns (GECs), might overcome the deficiencies. In the present study, the performance of GEC foundations in mitigating reverse faulting hazards was evaluated.

In this study, 1g model tests were conducted to investigate the performance of GEC foundations in mitigating the surface hazards associated with reverse faulting. For comparison, 1g model tests were also performed on unreinforced and GRS foundations. A 3-m thick foundation in prototype subjected to a reverse fault displacement up to 90 cm was modeled in the 1g model tests. The effectiveness of GEC foundations and the reinforcing mechanism of geotextile encasement in mitigating ground surface deformation was investigated. The key findings of this study provide valuable information that can be used by engineers to optimize the design of GEC foundations for mitigating reverse faulting hazards.

2 MODEL TESTS

2.1 *Test setup*

The 1g model tests on unreinforced, GRS, and GEC foundations were conducted using a sandbox in the geotechnical research laboratory at National Taiwan University. Figure 1 presents an illustration and overview image of the sandbox and test setup of the 1g model tests. The dimensions of the sandbox were 100 cm × 20 cm × 60 cm (length × width × height). Transparent plexiglass walls were installed on the front and back sides of the sandbox for visual observations during the tests. Thin plastic sheets with lubricant were applied to each plexiglass wall to minimize soil–wall interface friction. The bottom of the sandbox comprised a movable hanging wall and fixed footwall. Reverse fault displacement was generated by moving the hanging wall upward by using a driving motor installed under the sandbox. The initial location of the reverse fault tip was 58 cm from the left boundary, and the fault dip angle was set to 60° in this study.

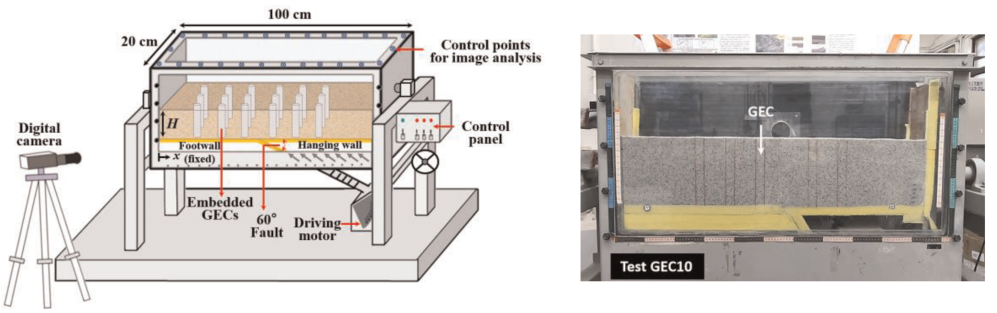

Figure 1. The sandbox and test setup: (a) illustration; (b) panorama.

2.2 *Material properties*

The soil and reinforcement materials used in the 1g model tests were carefully selected in accordance with the similitude requirements to ensure that the test models and the prototypes have comparable behavior. The material properties adopted in the 1g model tests were scaled down by using scaling factors derived in accordance with Buckingham's theorem

(Buckingham 1914). Table 1 summarizes all the scaling factors and the corresponding values in prototype for the model geometry and material properties. The soil material used in the 1g model tests was uniform quartz sand, which is classified as poorly graded sand (SP) according to the Unified Soil Classification System (USCS). The mean particle size of the test sand was D_{50} = 0.98 mm, and the target dry unit weight was γ_d = 15.3 kN/m^3 at a relative density D_r = 70%. The effective cohesion and peak friction angle of the test sand were c' = 0 kN/m2 and ϕ' = 39.2°, respectively, with confining pressures σ_3 ranged from 50 to 200 kPa; these values were obtained from triaxial consolidated–drained (CD) compression tests (ASTM D7181).

The reinforcement material used in the 1g model tests was nonwoven polypropylene geotextile. The ultimate tensile strength and failure strain of the nonwoven geotextile in the machine direction were T_{ult} = 0.7 kN/m and ε_f = 32.4%, respectively. The tensile stiffness of the nonwoven geotextile in the machine direction at the stress level of 50% of the ultimate tensile strength was J_{50} = 5.47 kN/m. For the geotextile encasement used in the GEC foundation test, the nonwoven geotextile in the designated machine direction was oriented along the circumferential direction of the geotextile encasement to develop hoop stress. The sand–geotextile interface friction angle was δ' = 27.4°, and the efficiency factor was calculated to be E_ϕ = tan δ'/tan ϕ' = 0.63.

Table 1. Scaling factors and values based on the similitude requirements.

Parameters	*Scaling factor	Model	Prototype
Geometry			
Foundation height, H (m)	$1/\lambda$	0.2	3.0
Soil parameter			
Target dry unit weight, γ_d (kN/m^3)	1	15.30	15.30
Friction angle, ϕ' (°)	1	39.2	39.2
Reinforcement parameter			
Ultimate tensile strength, T_{ult} (kN/m)	$1/\lambda^2$	0.70	157.5
Stiffness, J_{50} (kN/m)	$1/\lambda^2$	5.47	1231
Interface parameter			
Soil-geosynthetic friction angle, δ'	1	27.4	27.4

*Target scaling ratio λ= 15.

2.3 *Test models and digital image analyses*

The soil layer was constructed with a target relative density D_r = 70% by using the volume control method. In the GRS foundation test, a layer of planar geotextile was placed on a soil layer, and the process was repeated until the foundation reached H = 20 cm. Three layers of planar geotextile were placed in the foundation with a vertical spacing of S_v = 6.67 cm. In the GEC foundation tests, low-friction stainless steel tubes with lubricant were penetrated into a full-height soil layer (i.e., H = 20 cm) at the desired locations. The location of the outermost GEC installed in the footwall was determined by considering the influential zone of the free-field fault rupture. Each steel tube had a thin-walled tip to minimize its disturbance to the soil layer. The sand inside the steel tubes was extracted using a customized vacuum machine. The geotextile encasement was fabricated in advance and placed into the steel tubes, and the soil material was filled into the encasement and compacted to the target relative density. After the installation was completed, the steel tubes were carefully removed from the soil layer. A 1.5-cm thick soil layer was then constructed on the top of the GEC foundations to

provide overburden pressure. Figure 2 displays an illustration of the GEC foundation test. The diameter of the GECs was d_c = 3 cm, corresponding to a diameter of 0.45 m in prototype, and the length-to-diameter ratio of the GECs was l_c/d_c = 0.67. Fault displacement was generated after the test models were constructed, and the maximum fault displacement was set to S = 6 cm due to the limited displacement capacity of the sandbox. The ratio of fault displacement to foundation height was S/H = 30%.

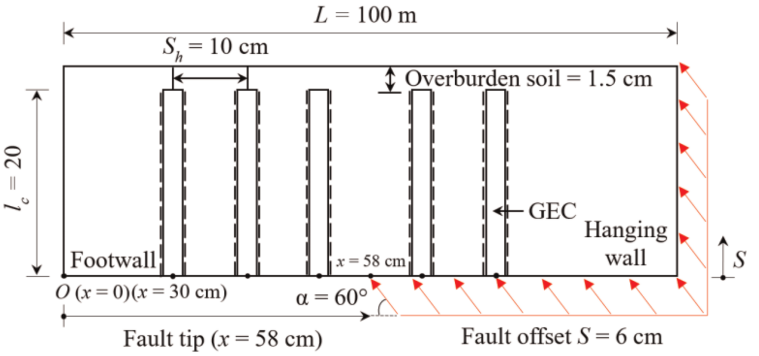

Figure 2. An illustration of the GEC foundation test (not in scale).

During the 1g model tests, charge-coupled device cameras, aimed at the front and top of the sandbox, were used for continuously monitoring the deformation of the test models. The recorded photographic data were analyzed using various digital image analysis (DIA) techniques to obtain the surface displacement profile, maximum angular distortion, and shear rupture propagation for the unreinforced, GRS, and GEC foundations at various fault offset magnitudes. Because the ground surface deformation induced by fault movement critically affects superstructure damage, the maximum angular distortion at the ground surface (β_{max}) was used as a key indicator in this study to evaluate the performance of the unreinforced, GRS, and GEC foundations. Details of the DIA techniques used in this study are provided in the paper of Yang *et al.* (2020).

3 RESULTS AND DISCUSSIONS

3.1 *Unreinforced foundation*

Figure 3a presents a series of test images of the unreinforced foundation subjected to reverse fault movement at fault offsets S = 1.5, 3, 4.5, and 6 cm. The test results indicate that the ground surface deformation became pronounced as the reverse fault displacement increased (Figure 3b). The β_{max} at the ground surface were 0.25, 0.76, 0.84, and 0.84 at S = 1.5, 3, 4.5, and 6 cm, respectively (Figure 3c). As expected, the β_{max} at the ground surface increased as the fault displacement increased and approached the slope of the peak friction angle of the sand ($\approx \tan\phi$ = 0.81) at large fault offsets. The fault influence length was L_I = 27.7 cm at S = 6 cm.

Figure 3d presents the shear strain contours of the unreinforced foundation subjected to reverse fault movement. The shear rupture propagated upward from the fault tip to the ground surface, and decreased in dip as it approached the ground surface. At S = 3 cm (S/H = 15%), the shear rupture broke through the foundation soil, and a surface fault rupture occurred at the ground surface. At this moment, the β_{max} at the ground surface considerably increased from 0.25 to 0.76 (Figure 6a), which indicated a high surface fault hazard risk.

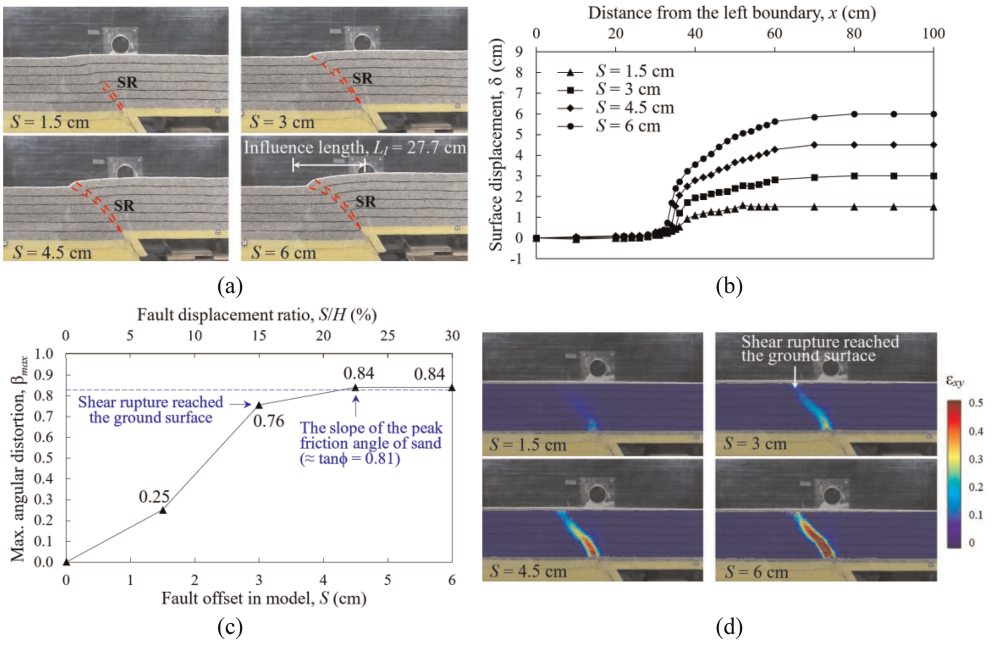

Figure 3. Results of the unreinforced foundation test (Test U) at various fault offsets: (a) test images; (b) surface displacement profiles; (c) maximum angular distortion; (d) shear strain contours.

3.2 *GRS foundation*

Figure 4a presents a series of test images of the GRS foundation subjected to reverse fault movement at fault offsets S = 1.5, 3, 4.5, and 6 cm. When reverse fault displacement occurred, the ground surface deformed in a similar manner to that of the unreinforced foundation (Figures 3b, 4b). The fault influence length was L_I = 22.1 cm at S = 6 cm, which is similar to the fault influence length for the unreinforced foundation (i.e., L_I = 27.7 cm). The β_{max} values were 0.18, 0.52, 0.74, and 0.84 at S = 1.5, 3, 4.5, and 6 cm, respectively (Figure 4c). The percentage reduction for β_{max} at S = 1.5, 3, 4.5, and 6 cm were R_d = 30.2%, 31.5%, 11.7%, and 0%, respectively, compared with the unreinforced foundation.

The test results revealed that the GRS foundation was effective in reducing β_{max} at relatively small fault offsets S = 1.5 and 3 cm (i.e., a fault displacement ratio $S/H < 15\%$). However, the effectiveness in reducing β_{max} decreased considerably after the shear rupture reached the ground surface (i.e., at S = 3 cm, as shown in Figure 4d). Similar shear strain contours were obtained for the unreinforced and GRS foundations (Figures 3d, 4d) because the mobilization of the reinforcement tensile strain was not developed when the hanging wall was moving upward (i.e., the GRS foundation was compressed).

3.3 *GEC foundation*

Figure 5a presents a series of test images of the GEC foundation subjected to reverse fault movement at various fault offsets. Stepped surface displacement profiles were observed as the reverse fault displacement increased (Figure 5b). The values of β_{max} were 0.17, 0.34, 0.59, and 0.64 at S = 1.5, 3, 4.5, and 6 cm, respectively (Figure 5c). Compared with the unreinforced foundation, the β_{max} at the ground surface significantly decreased. The percentage reductions for β_{max} at S = 1.5, 3, 4.5, and 6 cm were R_d = 33.3%, 55.6%, 30%, and 23.3%, respectively.

Figure 5d shows the shear strain contour for the GEC foundation subjected to reverse fault movement. Two reinforcing mechanisms, the shear rupture diffusion and diversion

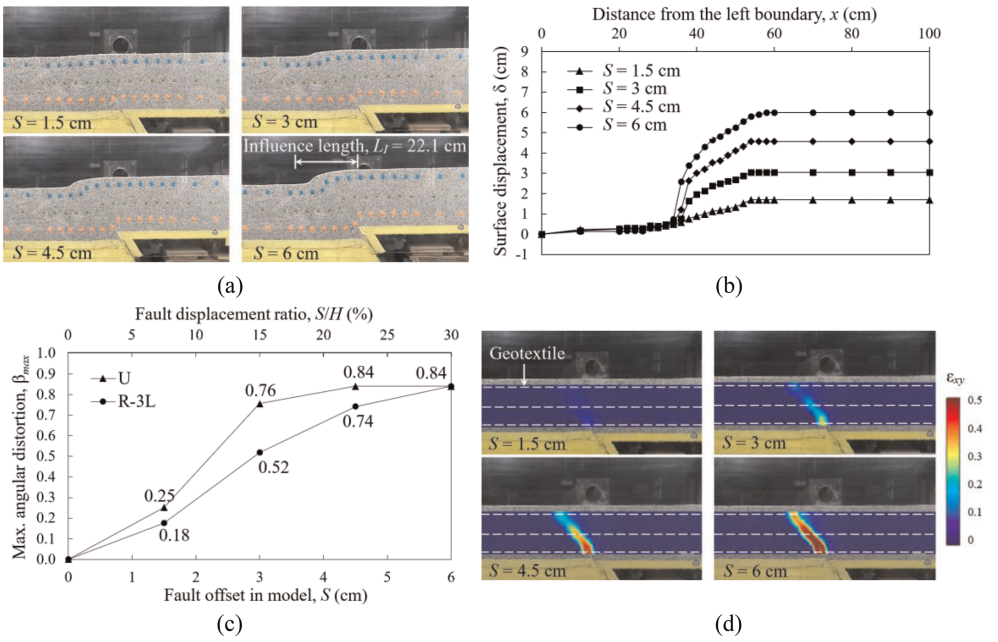

Figure 4. Results of the GRS foundation test (Test R-3L) at various fault offsets: (a) test images; (b) surface displacement profiles; (c) maximum angular distortion; (d) shear strain contours.

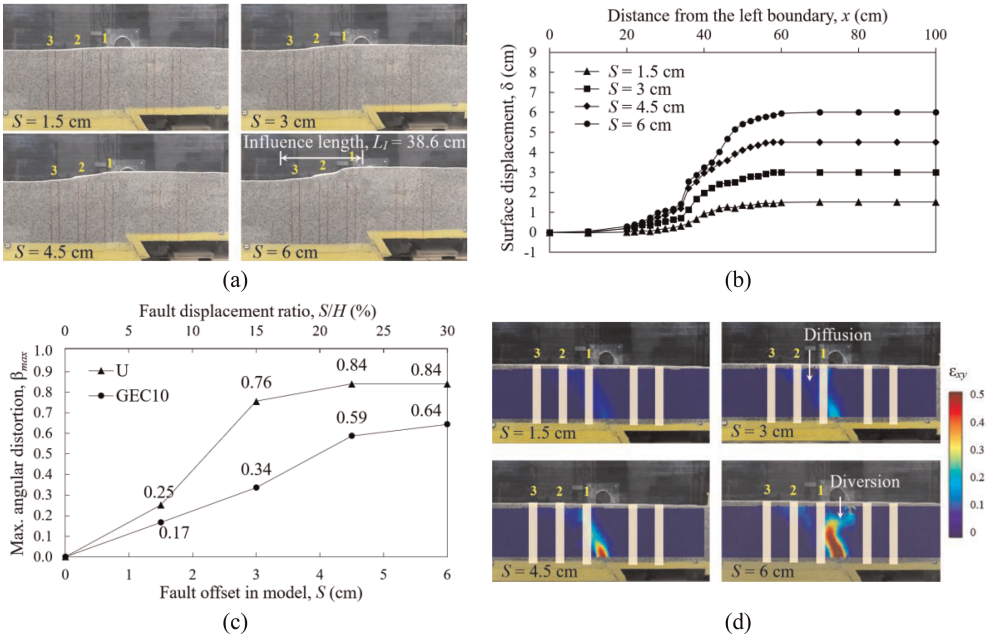

Figure 5. Results of the GEC foundation test (Test GEC10) at various fault offsets: (a) test images; (b) surface displacement profiles; (c) maximum angular distortion; (d) shear strain contours.

effects, were identified. When reverse fault displacement occurred, the fault-induced shear rupture propagated toward the first row of GECs placed in the footwall (indicated by 1 in Figure 5d). The fault-induced shear rupture diffused to the second and third rows of GECs (indicated by 2 and 3 in Figure 5d) during its propagation. The fault influence length was L_I = 38.6 cm at S = 6 cm, which is greater than the fault influence length for the unreinforced foundation (L_I = 27.7 cm). This result indicates that the mobilized tensile strain developed in the geotextile encasement, and the friction developed in the soil–geosynthetic interface effectively spread out the fault-induced shear rupture to a wider influential zone and further decreased the β_{max} at the ground surface. As the fault offset reached S = 6 cm (S/H = 30%), the fault-induced shear rupture was diverted toward the hanging wall, resulting in a considerable decrease in β_{max}. This diversion of the shear rupture was attributed to the increase in the lateral earth pressure acting on the GECs, enhancing the shear strength and bending stiffness of the GECs placed in the footwall. The increases in the shear strength and bending resistance of the GECs eventually diverted the fault-induced shear rupture.

4 CONCLUSIONS

The key findings of this study are as follows:

- For the unreinforced foundation, the β_{max} at the ground surface increased as the fault displacement increased and approached the slope of the peak friction angle of the sand at large fault offsets. At S = 3 cm (S/H = 15%), the shear rupture broke through the foundation soil, and a surface fault rupture occurred at the ground surface. At this moment, the β_{max} at the ground surface increased considerably, which indicated a high surface fault hazard risk.
- The GRS foundation was effective in reducing β_{max} at relatively small fault offsets. However, the GRS foundation was ineffective in reducing β_{max} after the fault-induced shear rupture reached the ground surface, with the R_d value decreasing to 0% at S = 6 cm (S/H = 30%).
- For the GEC foundation, stepped surface displacement profiles were observed as the reverse fault displacement increased. The β_{max} at the ground surface significantly decreased, with the percentage reduction for β_{max} ranging from R_d = 23.3%–55.6%. An R_d value of 23.3% was achieved as the fault offset reached 30% of the foundation height, which mitigates the risk of the surface fault hazards associated with large reverse fault movement. Two reinforcing mechanisms, the shear rupture diffusion and diversion effects, were identified.

REFERENCES

Buckingham, E. 1914. On Physically Similar Systems; Illustrations of the use of Dimensional Equations. *Physical Review* 4(4): 345–376.

Chen, Y.-G., Chen, W.-S., Lee, J.-C., Lee, Y.-H. & Lee, C.-T. 2001. Surface Rupture of 1999 Chi-Chi Earthquake Yields Insights on Active Tectonics of Central Taiwan. *Bulletin of the Seismological Society of America* 91(5): 977–985.

Chiang, J., Yang, K.-H., Chan, Y.-H. & Yuan, C.-L. 2021. Finite Element Analysis and Design Method of Geosynthetic-reinforced Soil Foundation Subjected to Normal Fault Movement. *Computers and Geotechnics* 139: 104412.

Yang, K.-H., Chiang, J., Lai, C.-W., Han, J. & Lin, M.-L. 2020. Performance of Geosynthetic-reinforced Soil Foundation Across a Normal Fault. *Geotextiles and Geomembranes* 48(3): 357–373.